On the Influence of gamma prime upon machining of advanced Nickel based superalloy

Zhirong Liao[a], Dragos Axinte[a,*] (1), Maxime Mieszala[b], Rachid M'Saoubi[c] (1), Ali Abelhafeez[a], Johann Michler[b], Mark Hardy[d]

[a] *Rolls-Royce UTC in Manufacturing and On-Wing Technology, Faculty of Engineering, University of Nottingham, UK*
[b] *EMPA, Swiss Federal Laboratories for Materials Testing and Research, Laboratory for Mechanics of Materials and Nanostructures, Thun, Switzerland*
[c] *Seco Tools AB, R&D Material and Technology Development, Fagersta, Sweden*
[d] *Rolls-Royce plc, Derby, UK*

Whilst gamma prime (γ') phase is the strengthening phase in Ni-based superalloys its influence on machining has been seldom investigated. This paper reports for the first time on the effect of γ' upon machining of Ni-based superalloys when cutting with parameters yielding different cutting temperature intervals which lead to strengthening/softening effects on the workpiece (sub)surface. In-depth XRD, SEM/FIB, EBSD analysis and unique micro-pillar testing in the workpiece superficial layers indicated that with the increase of γ' fraction the grain plastic deformation significantly decreased, while specific cutting energy can switch from low to high values influenced by the real cutting temperature.

Nickell Alloy, Machining, Gamma prime phase

1. Introduction

With the microstructure consisting of γ matrix and γ' precipitating and strengthening phase, Ni-based superalloys are widely used for the manufacture of safety critical components of aeroengines due to their high strength at elevated temperatures. This high performance is due to the significant volume fraction of γ' phase that stops the penetration of dislocations from γ constituent with its ordered L12 structure [1]. Thus, the development of these Ni-based superalloys is oriented towards high volume fractions of γ' (e.g. from ca. 25% of first generation to 60% for recent alloys respectively) to reach a set of optimum of mechanical properties (i.e. strength under high temperature) [2]. However, with the increase of γ' fraction, these alloys could display fast crack growth rates, which is an undesired effect. Consequently, when developing Ni-based superalloys for safety-critical applications, it is beneficial to achieve the desired strength performance with the minimum required volume fraction of γ' [3].

On the other hand, the machining defects (e.g. white layer, grain plastic deformation) are important factors that could influence the failure of the parts made of Ni-based superalloys [4-6]. However, the precipitation strengthening effect, which enhances the material tolerance to surface damage during machining, is only effective under a certain temperature range that when exceeded, can induce more material thermal softening thus inducing severer machining defects. This temperature range is highly dependent on the proportions of γ' (Fig. 1 [7]), where a high volume fraction of γ' yields a higher temperature range of strengthening effect.

While this dependency is exploited by material developers, limited information exists on the effect of γ' volume fraction upon workpiece surface integrity at microscopic level when machining.

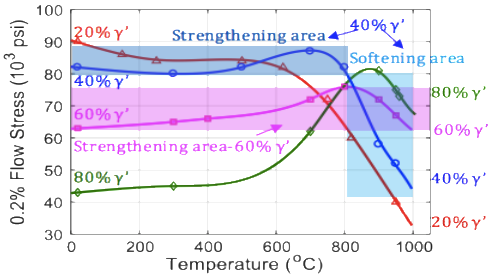

Fig. 1. Variation of the flow stress of Ni-based alloys with temperature for various proportions of γ'[7].

In this respect, this paper investigates for the first time on the influence of the γ' phase proportion upon the machinability and surface integrity of Ni-based superalloys. Due to the small range of the affected layer depth on the machined subsurface, e.g. grain deformation and recrystallizations, which are around/under tens of micrometres, advanced material investigation methodology, i.e. in-depth X-Ray diffraction (XRD), scanning electron microscope (SEM), focused ion beam (FIB), Electron backscatter diffraction (EBSD) analysis and state-of-the-art micro-pillar testing were employed to understand the phenomena governing the material microstructural evolution during the machining process.

2. Experimental approach and methodology

In this study, two Ni-based superalloys consisting of similar chemical composition (Table 1) but with different volume fraction of γ' (43% γ' and 57% γ' for alloys A and B, respectively) were investigated to enable the understanding of the influence of γ' phase upon the machining process. Powder compacts, about 76mm in diameter with can, were produced by hot isostatic pressing and heat treated to produce a fine grain microstructure.

Table 1 Chemical composition of the two Ni-based superalloys (wt%)

No.	Ni	Cr	Co	C	Mo	Zr	Nb	Ta	Al	Ti	B	Hf	W	Fe	Mn
A	Bal.	15	18.5	0.03	5	0.06	0	2	3	3.6	0.02	0.5	0.01	0.03	0
B	Bal.	12.3	4.0	0.03	0.6	0.06	2.1	4.6	3.8	2.6	0.02	0	3.1	3.4	0.5

Using advanced ion contrast channelling imaging it was revealed, both grain orientation and γ/γ' phase microstructure without chemical etching (Fig. 2). Similar grain size could be easily observed of these two different alloys while Alloy B shows more γ' phase under the high γ'/γ contrast imaging.

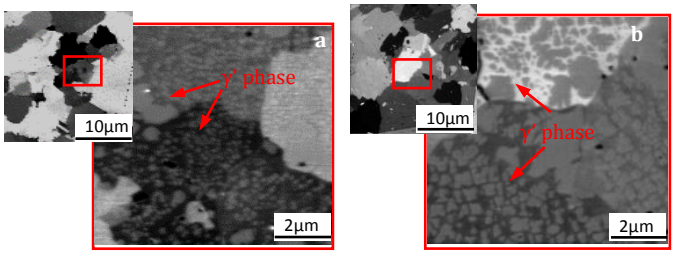

Fig. 2. Microstructure of (a) Alloy A (43% γ') and (b) B (57% γ') by advanced ion contrast channelling imaging.

Plunge turning were performed in orthogonal cutting mode using custom made Seco inserts (γ=0°, α=7°, 10μm edge radius) to study the machinability and surface integrity of these two alloys. Two cutting conditions yielding different cutting temperatures were used: (i) "normal conditions" with new tool and cutting speed vc=30m/min, feed rate f=0.1mm/rev; (ii) "aggressive conditions" with worn (VB=0.3mm) tool, vc=80m/min, f=0.1mm/rev. An Infrared CCD thermal camera was employed to measure the cutting temperature focusing on the cutting edge while dry cutting condition was employed to allow the temperature measurement.

The machined (sub) surface was studied with SEM following electrolytic etching with orthophosphoric acid. EBSD was also

applied with scanning step size of 0.5μm for deformed grain area and 0.05μm for recrystallized layer. A Proto XRD diffractometer was employed to measure the residual stress under the machined surface. To test the material strength within the machined subsurface, an advanced micro-pillar compression test (Alemnis) was applied in both the bulk material and machined edge.

3. Machinability investigation of two different alloys

3.1. Cutting temperature

Under normal cutting conditions both alloys yield similar cutting temperatures (max. 750°C) at the tool tip-workpiece contact area while under aggressive cutting condition it reached max. 950°C (Fig. 3). Due to the temperature dependence of γ' properties (Fig. 1), the flow stress of the two alloys yielded different strengthening /softening effects correspondingly. For Alloy A (43% γ'), within normal cutting condition the max. cutting temperature (750 °C) is still in the strengthening effect zone (Fig. 1), while the material is softened significantly during aggressive cutting where the maximum cutting temperature reached 950°C. However, at this cutting temperature zone (700-950°C) Alloy B (57% γ') is mainly under strengthening condition, which is around the peak point of the stress while the softening effect could be neglected. Thus, in aggressive cutting conditions, although similar temperature is achieved, the Alloy A and B are in totally different strength status.

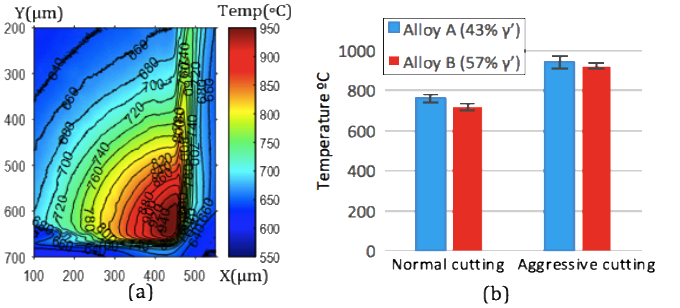

Fig. 3. (a) Example of temperature map (aggressive cutting) and (b) max. cutting temperatures at the tool-workpiece interface (error bars – 1Stdev).

3.2. Specific cutting energy

The specific cutting energy (SCE), Eq. 1 [8,9], for which cutting temperature is an indicator, could be used to evaluate the machinability of these two alloys:

$$E = E_s + E_f + E_p = \frac{F_s}{A_s} \cdot \frac{\cos\gamma}{\sin\emptyset\cos(\emptyset-\gamma)} + \frac{F_n \sin\gamma + F_c\cos\gamma}{bh_c} + \frac{F_p V_s}{hfV_c} \quad (1)$$

where: E, E_s, E_f, E_p - total, shear, friction and ploughing specific energy; F_s, F_c, F_n, F_p - shearing, cutting, normal cutting and ploughing force; ϕ - shear angle; A_s and V_s - shear area and cutting speed; b, h and h_c - cutting width, undeform and deformed chip thickness; these parameters can be measured or calculated [8,9].

As shown in Fig. 4, the SCE mainly stems from the contribution of friction and shear energy while the ploughing energy is low compared with others due to the applied small edge hone (10μm).

Under normal cutting condition, the SCE of Alloy A (43% γ') is similar to Alloy B (57% γ'). This is because under these conditions the cutting temperature of both alloys is max. 750 °C where both alloys are under strengthening effect (region <800°C - Fig.1).

Under aggressive cutting conditions, it is interesting to see the specific friction energies (SFE) of both alloys are similar while the specific shear (SSE) and total energy of Alloy A (43% γ') are much lower than Alloy B (57% γ'). This is because under high cutting temperature (region >800°C-Fig.1) the material flow stress of Alloy A is reduced due to softening effect while Alloy B is still in strengthening condition, leading to higher SSE while the SFE is the same since both friction coefficients did not change significantly.

Observing the influence on cutting temperature and specific machining energy from the changes of volume fractions of γ', it can be expected that the surface integrity of machined workpiece will be affected significantly as a result. This leads to the need of study on the microstructural phenomena occurring at micrometric level.

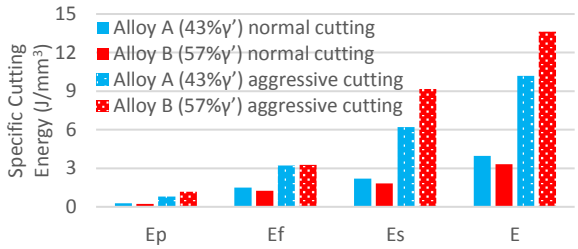

Fig. 4. Specific energies of two alloys under different cutting conditions.

4. Surface integrity impact from the changing of γ' phase.

4.1. Metallographic study

Fig. 5a, b shows SEM images of machined subsurface in normal cutting conditions where both alloys present similar level of material drag (ca. 6μm) while in aggressive cutting conditions (Fig. 5c, d) they display comparable (ca. 4μm) level of recrystallized layer (white layer). However, it is surprising to find in aggressive cutting condition that Alloy A shows higher level of material drag under the white layer while Alloy B shows nearly no material drag under this condition. This is because at normal cutting condition both alloys were under the temperature zone yielding material strengthening which leads to similar level of material drag. On the other hand, under aggressive machining condition high cutting temperature (950°C) was reached, where the Alloy A shows softening effect due to lower γ' fraction, while Alloy B was still under strengthening stage because of higher γ' fraction. Thus, although the recrystallization occurred in both alloys on the machined surface, subsurface grains in Alloy B retained higher deformation resistance than Alloy A.

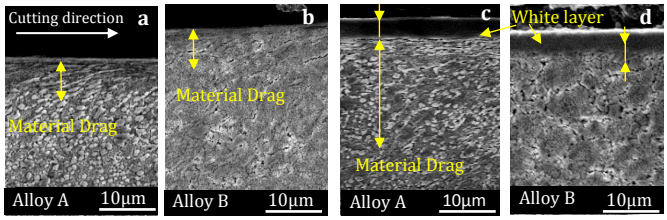

Fig. 5. SEM image of subsurface under normal (a and b) and aggressive cutting conditions (c and d) for Alloy A (43% γ') and Alloy B (57% γ').

4.2. Grain evolution revealing the subsurface damage mechanism

In order to identify the damage mechanism of the machined subsurface under different cutting conditions, the inverse pole figures (IPF) from EBSD mapping were obtained (Fig. 6) where grain deformation and intragranular rotation near the machined surface was revealed. This effect is especially significant in Fig. 6(c) in which the Alloy A (43% γ') is greatly softened under high cutting temperature with aggressive cutting condition leading to also high level of material drag (Fig. 5c). On the contrary, under the same aggressive cutting condition, Alloy B (57% γ'- Fig. 6d) shows much less grain deformation and intragranular rotation in subsurface due to its larger strengthening range with high γ' precipitation hardening. Under aggressive cutting, a clear evidence of recrystallization with much smaller grain size (~0.5μm) happened near the machined surface (Fig. 6e, f) compared with parent grain (~5μm); for normal cutting the grain size just reduced ca. 15% due to grain deformation (see Table 2 for all grain size information).

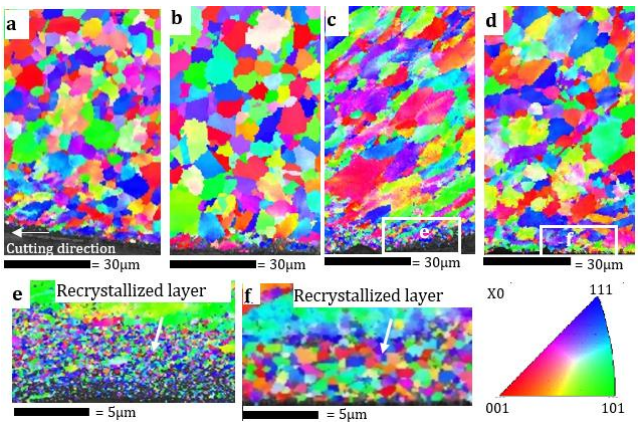

Fig. 6. EBSD images near machined surface for normal cutting of Alloy A (a) and Alloy B (b) and aggressive cutting of Alloy A (c, e) and Alloy B (d, f)

Table 2 Average grain size of the alloys under different cutting conditions

Material	Alloy A (43% γ')			Alloy B (57% γ')		
	Bulk area	Normal cut	Aggressive cut	Bulk area	Normal cut	Aggressive cut
Average grain size (μm)	4.6	3.95	0.31	5.4	4.5	0.67

To evaluate the extent of microscale plastic strain in the machined subsurface, the microstructural local misorientation (LMO) was mapped by displaying small orientation changes in the lattice under 5° subgrain angle (Fig. 7), which is related to the dislocations accumulated in the crystal during grain deformation. Under normal cutting condition both show similar LMO contouring where a near surface extent of high strain area was observed. More interestingly, in aggressive cutting condition the Alloy A shows a much higher effect of plasticity upon the crystallite lattice than Alloy B, indicative of a severer material dislocation activity and higher plastic strain behaviour in the machined subsurface.

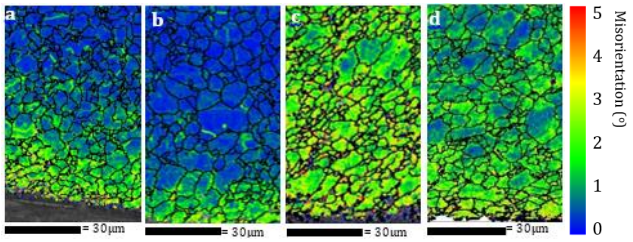

Fig. 7. Local misorentation maps of subsurface with normal cutting of Alloy A (a) and B (b) and aggressive cutting of Alloy A (c) and B (d).

To quantify the extent of plastic strain of the machined subsurface, a modified average intragranular misorientation (AMIS) is used [4]. Within each of M grains scanned by a line of N points, the modified AMIS can be calculated in Eq. 2, where θ_{jk} is the misorientation between points j and k within grain *i*.

$$AMIS = \frac{\sum_{i=1}^{M}\left(\frac{2\sum_{j=2}^{N}\sum_{k=1}^{j}\theta_{jk}}{N_i(N_i-1)}\right)_{grain(i)}}{M} \quad (2)$$

In Fig. 8, the extent of surface damage is indicated by the AMIS profiles as a function of depth from the machined surface, where under normal cutting condition Alloy A displays a slightly higher AMIS compared with Alloy B while both of them showing much lower value compared with aggressive cutting condition and the strengthening effect could be verified. It is not surprising that under aggressive cutting condition the Alloy B shows a faster decrease than Alloy A away from the machined layer but it is interesting to see near the machined surface (<10μm) both show the same values where the recrystallization occurs. On the other hand, considering the observation in previous section that high cutting temperature happened in aggressive cutting condition, it could be concluded that the white layer is generated under high temperature and high plastic strain to reach the nucleation of material recrystallization.

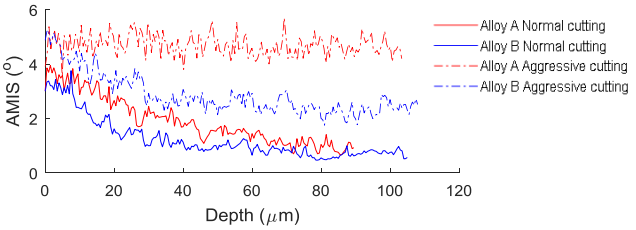

Fig. 8. Average intragranular misorientation profile as a function of depth from the machined surface.

5. Mechanical characteristics of machined subsurface layers

5.1. Subsurface work hardening and residual stress analysis

The results of residual stress and subsurface work hardening depth (obtained from XRD analysis and microhardness measurement, respectively) are depicted in Fig. 9. Alloy A exhibits ~20% higher surface residual stresses and ~15% higher depth of work hardened layer compared to Alloy B under aggressive cutting condition while in normal cutting condition shows slightly higher/similar values, which is somehow also correlated to the grain deformation condition. Moreover, the residual stress decreases to 0MPa at a depth of 150μm and 250μm under normal and aggressive cutting respectively, showing a reasonable agreement with the resulting work hardening depth.

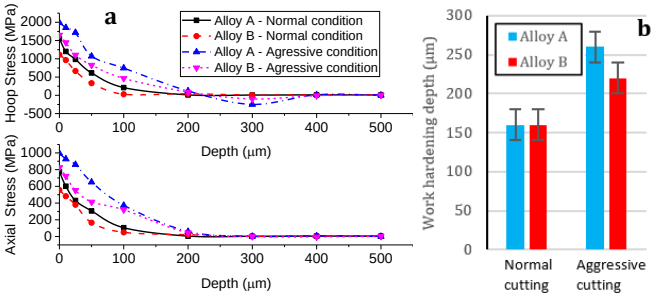

Fig. 9. Residual stress distribution (a) and work hardening depth (b).

5.2. Micropillar test for yield stress analysis in the machined surface

The previous analysis shows clearly phenomena of grain deformation and refinement occurring selectively depending on γ' fraction and temperature in the machined subsurface during cutting which, consequently, influence the material strength.

However, due to the small thickness (microns) of affected layers, up to now, their mechanical properties have been obtained only through conventional nano-indentation methods [5]. To study the material strength evolution during the machining process, this paper employed for the first time a state-of-the-art micro-pillar testing on the machined subsurface. The micropillars were prepared near the machined surface (<2 μm from micropillar centre to surface) and the bulk material in the axial direction with a diameter of 3μm and a height of 9 μm (i.e. an aspect ratio of 3:1), by using a Tescan dual FIB/SEM. For each sample at least 4 pillars were tested. Experiments were conducted on an Alemnis nanoindenter equipped with a diamond flat punch at a constant strain rate of ~10^{-3}/s and under room temperature. The Sneddon's correction was applied to take into account the compliance of the Ni substrate. Fig. 10 shows, as examples, the micropillars in the bulk material and near the machined surface (edge) obtained with aggressive cutting on Alloy A. By combining ion contrast channelling imaging, the micropillar in bulk material shows big grain size (3 grains in a pillar – Fig. 10a) while the edge area obtained with aggressive cutting shows a multitude of small grains (Fig. 10b); no such evidence has been presented before.

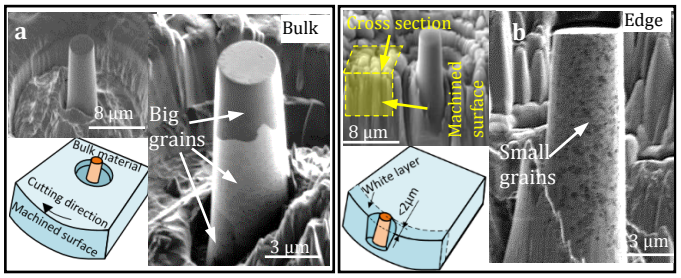

Fig. 10. Preparation of micropillars with grains being observed: bulk material (a) and near the machined surface within white layer (b).

Fig. 11 shows the representative stress–strain curves of micropillar compression tested. It can be seen: (i) at the beginning of compression all curves show a steep slope due to the compressing deformation and (ii) later in bulk material and normal cutting the slopes following a mitigating tendency corresponding to a slipping failure of micropillar while in aggressive cutting the slopes keep increasing with the strain, corresponding to a buckling failure and showing higher strain hardening. This is the first time the micrometric level mechanical properties of white layer are presented: clearly Fig.12 shows that while the micropillar in white layer is prone to buckling failure, in the material drag layer and bulk material the micropillars fail by slippage. This enhances the evidence of work hardening on recrystallized layer and quantifies the yield strength (Table 3).

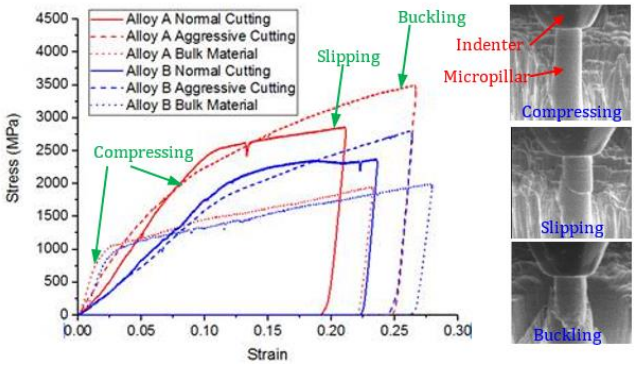

Fig. 11. Micropillars compression test showing different deformations.

Table 3 Yield strength of two alloys under different cutting conditions

Material	Cutting condition		Yield strength (MPa) Tensile test 0.2%	Yield strength (MPa) Micropillar Compression test 1%
Alloy A (43% γ')	Bulk material		1011	961±96
	Superficial layer	Normal cut	-	2349±266
		Aggressive cut	-	2121±235
Alloy B (57% γ')	Bulk material		1053	970±81
	Superficial layer	Normal cut	-	2040±142
		Aggressive cut	-	1797±82

From Fig. 11 and Table 3, it can be seen that in bulk material both alloys show similar yield strength under micropillar compression test and normal tensile test. Compared to the bulk counterparts the yield strengths of the micropillars at the near machined surface were increased by 144% and 120% within Alloy A under normal cutting and aggressive cutting respectively, while Alloy B was increased only 110% and 85% correspondingly. This shows the effect of higher strengthening effect on Alloy B under high cutting temperate which leads to lower dislocation and work hardening on the subsurface which results in higher surface integrity. When comparing both cutting conditions, the yield strength in the aggressive cutting conditions appears to be lower by 9% for Alloy A and by 11% for the Alloy B respectively, due to the recrystallization of white layer which containing small grain size that leads to buckling failure of micropillars.

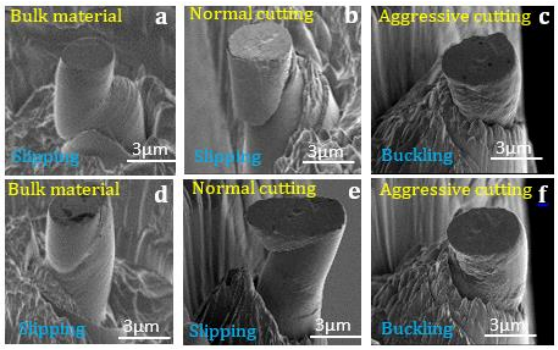

Fig. 12. Compressed micropillars: Alloy A (a- c) and Alloy B (d-f).

6. Conclusion

This paper reports for the first time on the influence of changing the volume fraction of γ' phase proportion upon the machinability and surface integrity of Ni-based superalloy. An in-depth investigation on orthogonal turning with advanced mechanical and metallurgical analysis was reported. The results indicated that with normal cutting condition both low (43%) and high (57%) γ' alloys output similar cutting temperatures (~750°C) and surface integrity while low γ' alloy resulted in a slightly higher level of strain contour on the subsurface. Under aggressive cutting conditions both alloys reached a high cutting temperature (~950°C) where the low γ' alloy is subject to a softening effect and resulting in lower cutting energy but more severe surface damage when compared with high γ' alloy. By use of unique micropillar compression tests, the superficial (recrystallized, dragged) layers generated during machining Ni-based superalloys have been evaluated for their yield strength, thus giving more understanding on the nature of resulting surface integrity.

These studies conclude that the high γ' fraction alloy, equipped a better strengthening effect under high cutting temperate, outputs a better surface integrity but lower machinability. Further, this study also highlights the possibility to understand the machinability and subsequent surface integrity of the new Ni-based superalloys even from their design stages.

Acknowledgement

The authors would like to thank Rolls-Royce plc. for provision of material and financial support on this research.

References

[1] Francis M, et al (2014) High-temperature deformation mechanisms in Ni-base alloy studied by neutron diffraction and electron microscopy. Acta Mater. 74: 18-29.
[2] Vattré, A, et al (2009) Dislocation dynamics simulations of precipitation hardening in Ni-based superalloys with high γ' volume fraction. Intermetallics 17(12): 988-994.
[3] Hardy C, et al (2004) Developing damage tolerance and creep resistance in a high strength nickel alloy for disc applications. Superalloys 2004: 83-90.
[4] M'Saoubi R, et al (2012) Surface Integrity Analysis of Machined Inconel 718 Over Multiple Length Scales. Annals of the CIRP 61(1):99–102
[5] M'Saoubi, R, et al (2014) Surface integrity of nickel-based alloys subjected to severe plastic deformation by abusive drilling. Annals of the CIRP 63(1): 61-64.
[6] M'Saoubi R, et al (2015) High performance cutting of advanced aerospace alloys and composite materials. Annals of the CIRP 64(2): 557-580.
[7] Breadmore P, et al (1969) On temperature dependence of flow stress of Nickel-base alloys. Metallurgical Society of AIME-Transacation 245 (7):1537-1545.
[8] Shaw C, Metal cutting principles. Vol. 2. New York: Oxford university press, 2005.
[9] Manjunathaiah J, et al (2000) A new model and analysis of orthogonal machining with an edge-radiused tool. J. Manuf. Sci. Eng.-Trans. ASME 1001: 48109-2125.